Sensory domain contraction in histidine kinase CitA triggers transmembrane signaling in the membrane-bound sensor

Michele Salvi[a,1], Benjamin Schomburg[a,1], Karin Giller[a], Sabrina Graf[b], Gottfried Unden[b], Stefan Becker[a], Adam Lange[a,2,3], and Christian Griesinger[a,3]

[a]Department of NMR-based Structural Biology, Max Planck Institute for Biophysical Chemistry, 37077 Gottingen, Germany; and [b]Institute for Microbiology and Wine Research, Johannes Gutenberg University of Mainz, 55128 Mainz, Germany

Bacteria use membrane-integral sensor histidine kinases (HK) to perceive stimuli and transduce signals from the environment to the cytosol. Information on how the signal is transmitted across the membrane by HKs is still scarce. Combining both liquid- and solid-state NMR, we demonstrate that structural rearrangements in the extracytoplasmic, citrate-sensing Per-Arnt-Sim (PAS) domain of HK CitA are identical for the isolated domain in solution and in a longer construct containing the membrane-embedded HK and lacking only the kinase core. We show that upon citrate binding, the PAS domain contracts, resulting in a shortening of the C-terminal β-strand. We demonstrate that this contraction of the PAS domain, which is well characterized for the isolated domain, is the signal transmitted to the transmembrane (TM) helices in a CitA construct in liposomes. Putting the extracytoplasmic PAS domain into context of the membrane-embedded CitA construct slows down citrate-binding kinetics by at least a factor of 60, confirming that TM helix motions are linked to the citrate-binding event. Our results are confirmation of a hallmark of the HK signal transduction mechanism with atomic resolution on a full-length construct lacking only the kinase core domain.

transmembrane receptors | solid-state NMR spectroscopy | transmembrane signaling | integrated structural biology | histidine sensor kinase

H istidine kinases (HKs) are key players in prokaryotic signaling and the primary means of processing extracellular stimuli (1–6). Due to their modular organization, HKs can relay a multitude of different input stimuli, including sensing of nutrients, light, physicochemical parameters (e.g., metal ions, ions gradient), temperature, oxygen, and molecules reporting cell density, to accomplish diverse responses. Over the last decade, various structures have been solved for the cytosolic kinase core and a number of signaling domains and more recently even for the complete cytoplasmic region (7–13), but the transmembrane (TM) signaling mechanism itself remains challenging to decipher. Structural information on individual stimulus-receiving domains therefore provides an important tool to identify TM signal transduction schemes.

Because extracytoplasmic receiver domains are generally directly connected to TM helices, structural rearrangements within these motifs can be correlated with the TM-signaling mechanism. Different receiver domains have been characterized with and without their ligands and reveal structural differences between the two states that impose restraints on possible motions of the TM helices. Based on such structures, a symmetry-to-asymmetry switch has been postulated for KinB (14), TorT/TorS (15), and LuxPQ (16), implying a possible tilt of TM helices (17). For chemotaxis sensor Tar and for HK NarX a piston movement of the second TM helix has been postulated as a consequence of receiver domain motions (9, 18–20).

Among receiver domains, PAS domains stand out by being able to process diverse input signals, which is reflected by their abundance (9). Depending on their ligands, PAS domains have

been associated with a piston-type motion (21–23) or a scissors-like displacement of TM helices (24) for signaling across the membrane. However, structures of full-length HKs including TM regions are so far not available. No doubt, also partial structures of HKs, especially those comprising several domains like the complete cytoplasmic regions of VicK and YF1 (13, 25), have been instrumental for developing mechanistic models of signal transduction in HKs. However, establishing the relevance of structural findings in such isolated, soluble domains regarding the mechanism of TM signaling in native HKs is mandatory to confirm mechanistic models. Previous findings from our laboratory demonstrate a contraction of the citrate-sensing PAS domain (PASp = periplasmic PAS domain) of HK CitA from *Klebsiella pneumoniae* (Kp CitA) upon citrate binding, inducing a pull on the C-terminal β-strand (β5) leading into the second TM helix (TM2) (23). Combining liquid- and solid-state NMR experiments, we have now been able to confirm these structural rearrangements in CitA from *Geobacillus thermodenitrificans* in context of the TM helices.

Results

Citrate Responsiveness and Selectivity of *G. thermodenitrificans* CitA. To investigate citrate-free and citrate-bound states of CitA from the thermophile *G. thermodenitrificans*, we characterized the

Significance

Histidine kinases are key players in prokaryotic environment sensing. Citrate binding to the extracytoplasmic sensing domain of histidine kinase CitA triggers a contraction of the domain, resulting in a pull on the C-terminal β-strand. By a combination of liquid- and solid-state NMR spectroscopy, structural alterations observed for the isolated domain can be confirmed in context of its native environment as part of a membrane-embedded receptor. Our results demonstrate that the mechanistic model derived from the isolated ligand-sensing domain is compatible with the sensor in a native-like membrane environment and allows transfer of the model to transmembrane signaling by this class of sensor kinases.

isolated PASp domain in solution (CitA PASp$_{free}$ and CitA PASp$_{bound}$) and in liposome-embedded constructs comprising both the extracytoplasmic and cytosolic PAS domains as well as the TM helices (CitApc = full HK without the kinase core domain) (Fig. 1A). The reduction of CitA to the CitApc and the PASp domain constructs is justified as essential structural and binding properties are conserved in these constructs. This approach was previously used on the dicarboxylate receptor DcuS, another HK from the CitA family (26). However, we could not establish the mechanism for this HK because the ligand-free construct was not experimentally accessible (8, 27). First, *G. thermodenitrificans* CitA (Gt CitA, i.e., the complete HK) was characterized functionally. Citrate responsiveness and selectivity of Gt CitA was monitored by CitA-CitB receptor-dependent activity using a reporter gene assay as described previously for *Escherichia coli* DcuS (Ec DcuS) (26, 28). Gt CitA was shown to be able to restore the CitA-CitB two-component system in a CitA-deficient *E. coli* strain in a citrate-dependent manner (Fig. 1B). Surprisingly, isolated Gt CitA PASp did not show any citrate-binding effect when monitored by NMR. As full-length CitA was functional in vivo, we hypothesized that the lack of responsiveness might be due to tight ligand binding, resulting in citrate being bound before titration. In the crystal structure of the citrate-bound PASp domain of Kp CitA (PDB entry: 2J80; release date, October 23, 2007), arginine R101 interacts directly with the ligand, as shown in *SI Appendix*, Fig. S5 (23). In a BLAST sequence alignment (29) this residue is highly conserved (30). The homologous Gt CitA PASp (R93A) mutant was citrate-responsive in solution. Moreover, full-length CitA (R93A)
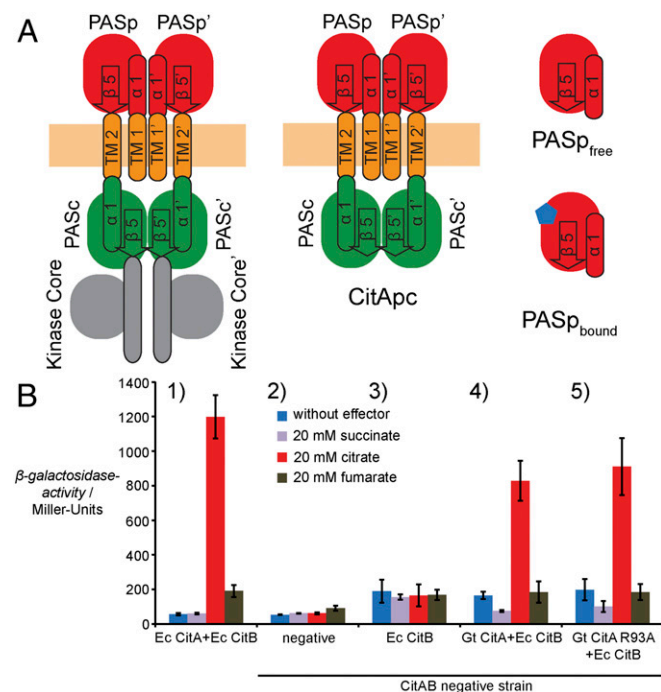

Fig. 1. Construct design and activity of CitA. (A) Constructs of CitA used in structural studies. *Left* to *Right*: Full-length CitA, CitApc without kinase core (solid-state NMR), isolated PASp with and without citrate (blue pentagon) used in liquid-state NMR. (B) Activity of CitA in a complementation assay. The activity of response regulator CitB of *E. coli* (Ec) was monitored as a function of ligand input. Whereas complementation of a CitA/CitB-negative strain (IMW549) of *E. coli* (panel 2) with plasmid-encoded CitB alone is inactive (panel 3), complementation with *G. thermodenitrificans* (Gt) CitA (pMW or CitAR93A) and *E. coli* CitB restores citrate-induced, selective response (panels 4 and 5, respectively), very similar to the activity in strain IMW548 of *E. coli* that is wild-typic for CitA/CitB (panel 1).
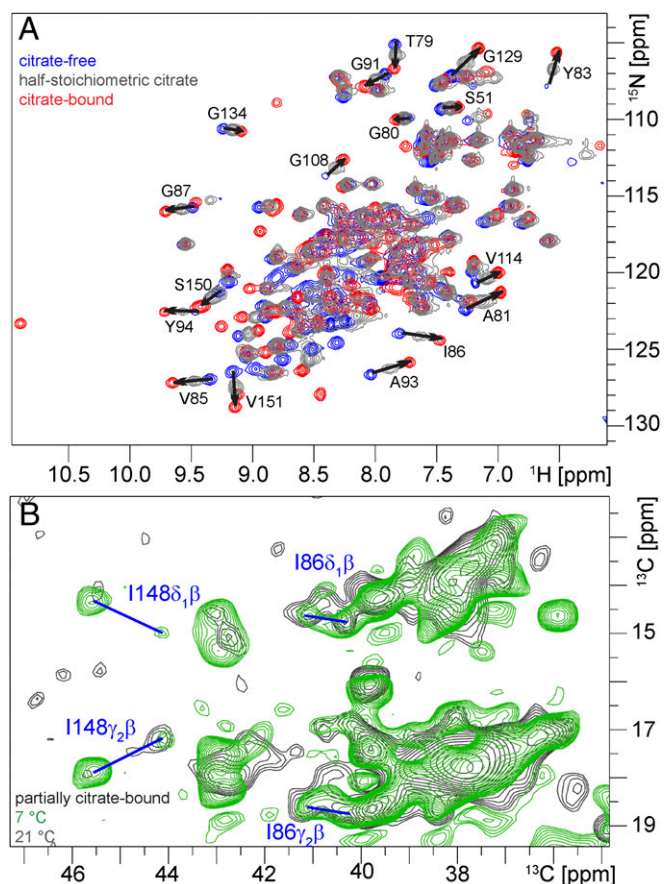
Fig. 2. Citrate-binding kinetics of PASp in isolation and in CitApc. (A) The ^{15}N-HSQC citrate titration of PASp (R93A). Spectra were recorded on a 400-MHz spectrometer at 25 °C. Three representative data points [citrate-free, half-stoichiometric, and saturated PASp (R93A)] are shown. The appearance of intermediate peaks during the titration is indicative of fast protein/ligand exchange. Shifts for isolated peaks are highlighted, denoting the respective residues. The exchange rate of ligand-free and -bound states was determined from the I86 trace. (B) The 20-ms PDSD spectra of CitApc (R93A) with substoichiometric citrate (detail of the isoleucine side-chain region is shown) were recorded on an 850-MHz spectrometer at 7 °C (green) and 21 °C (gray). Instead of intermediate peaks, two sets of signals for citrate-free and citrate-bound PASp appear (chemical shift difference between both states is highlighted as lines), suggesting slow protein/ligand exchange in context of TM helices. The upper limit for exchange rates was determined from I86 Cδ_1-Cβ peaks on the Cδ_1 resonances in ω_1.

also proved to function like wild-type protein in vivo as shown by a reporter gene assay (Fig. 1B). By global fitting based on 42 isolated proton shift assignments from an NMR titration curve (*SI Appendix*, Fig. S2), using the equation reported in ref. 31, a K_d of 640 ± 21 μM was determined (32, 33), showing fast exchange kinetics between free and bound forms (Fig. 2). Other potential ligands like fumarate, malate, or succinate did not have any effect on NMR spectra (*SI Appendix*, Fig. S1). Whereas the ligand affinity of PASp (R93A) is two orders of magnitude weaker than for *K. pneumoniae* CitA (Kp CitA) (34), it is still stronger than the K_d reported for DcuS toward its ligands (27).

Structure of both Signaling States of CitA PASp (R93A). Because it turned out to be impossible to obtain the citrate-free form of wild-type Gt CitA PASp, the validity of Gt CitA PASp (R93A) structures as functional receiver domain states has to be established by comparison with the known structures of PASp domains in their citrate-free and -bound forms. Based on liquid-state NMR
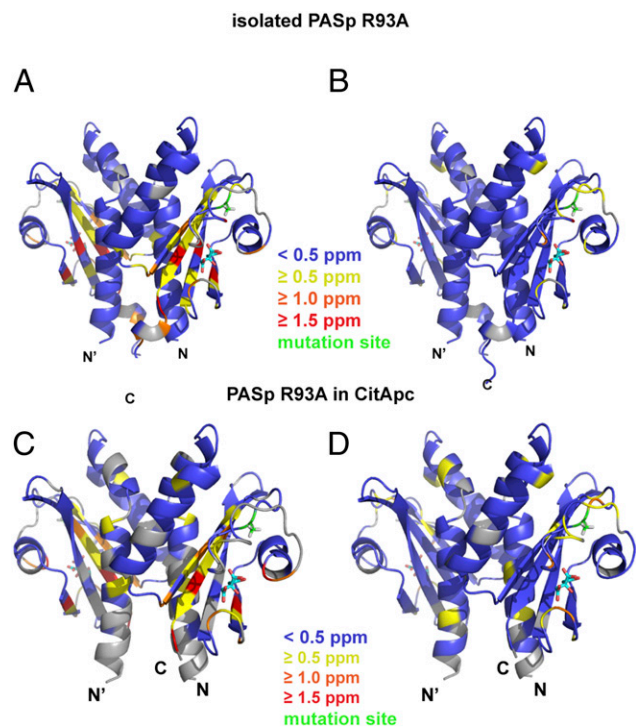
Fig. 3. Citrate-binding effects on PASp. (*A*) Cα-Cβ chemical shift differences between PASp (R93A)$_{free}$ and PASp (R93A)$_{bound}$ mapped on the NMR structure of PASp R93A$_{bound}$ aligned with the Kp CitA PASp crystal structure dimer (23). Mutation site R93A is shown in green, unassigned residues in gray. From blue to red: increasing degree of chemical shift perturbation. (*B*) Cα-Cβ chemical shift differences between PASp (R93A)$_{bound}$ and wild-type PASp$_{bound}$. (*C*) Cα-Cβ chemical shift differences between PASp (R93A) (citrate-free) and PASp (R93A) (citrate-bound) in membrane-embedded CitApc. (*D*) Cα-Cβ chemical shift differences between PASp (R93A) (citrate-bound) and wild-type PASp (citrate-bound) in membrane-embedded CitApc.

assignments, the secondary structure of each residue was deduced from carbon chemical shifts (35). Structural features can in addition be compared with NOE-derived structures of Gt CitA PASp (R93A)$_{free}$ and PASp (R93A)$_{bound}$ (*SI Appendix*, Table S1 and *SI Appendix*, Fig. S3 *A* and *B*) and to Kp CitA PASp crystal structures (23), which we used as a reference. First, based on chemical shift analysis, structural elements of the PAS-fold as found in Kp CitA (23) were confirmed in Gt CitA PASp (R93A)$_{free}$ and (R93A)$_{bound}$ (*SI Appendix*, Fig. S3 *C* and *D*); furthermore, structural differences between the two R93A samples were tracked through Cα-Cβ chemical shift changes. In general, the whole central β-scaffold of PASp is affected by citrate binding (Fig. 3*A* and *SI Appendix*, Fig. S3*A*). Comparison of the Cα-Cβ chemical shifts between wild-type PASp and PASp (R93A)$_{bound}$ reveals only minor differences, confirming that wild-type PASp indeed is in a citrate-bound state (Fig. 3*B*).

An interesting finding based on the secondary structure analysis is the shortening of the C-terminal β-strand of PASp (R93A) upon citrate binding. At L154, a transition from negative secondary shift, indicative of β-strand conformation (35), to positive secondary shift in the citrate-bound state is observed (Fig. 4*A*). Based on sequence alignment, L154 is found to be at the exact position of T128 in Kp CitA (Fig. 4*C*), the residue switching from β-sheet conformation in the citrate-free state to non–β-sheet conformation upon citrate binding within this PASp homolog. The secondary structure alterations in Gt CitA PASp are thus in agreement with earlier findings for the isolated extracytoplasmic domain of Kp CitA (23). The NMR structures of Gt CitA PASp (R93A) compare well with the Kp CitA PASp

crystal structures, with backbone rmsd of 2.1 Å and 1.8 Å for the citrate-free and citrate-bound states, respectively. The shortening of the C-terminal β-strand and the apparent increased propensity for helix formation of residues at the C terminus in the citrate-bound state is common to both homologs (*SI Appendix*, Fig. S3 *C* and *D*).
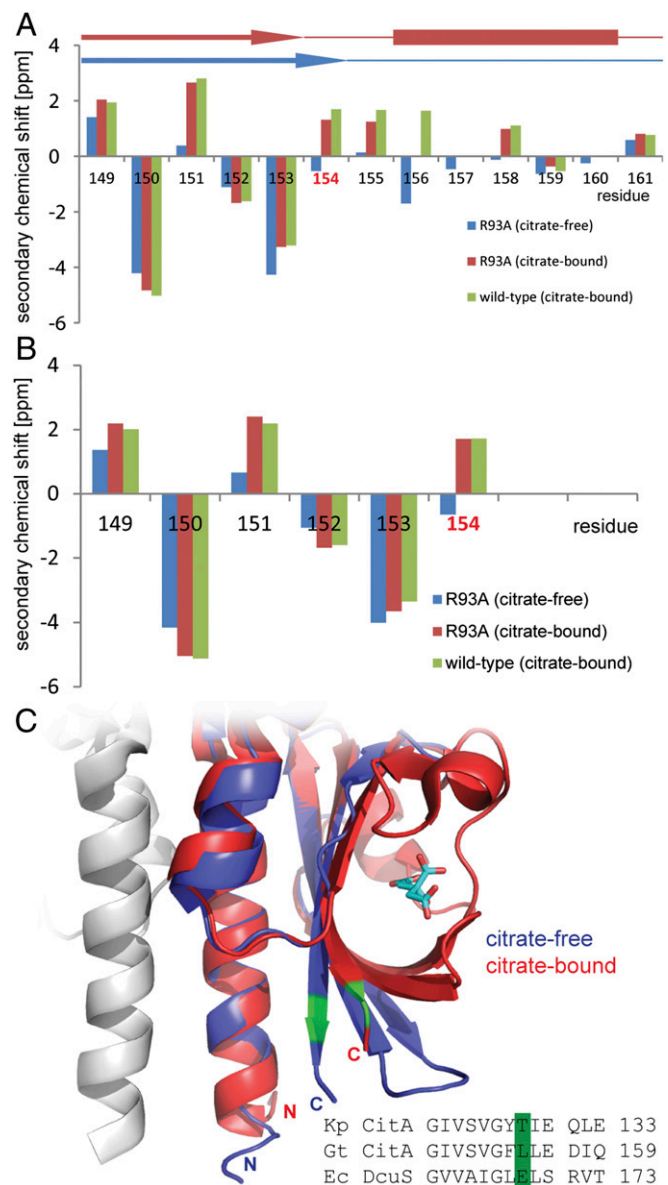
Fig. 4. Citrate-binding induces secondary structure switch L154. (*A*) Cα-Cβ secondary chemical shift plot for the C terminus of wild-type PASp and PASp (R93A) in citrate-free and -bound states. At L154, a secondary shift sign change is induced by citrate binding. The secondary structure elements shown above the plot were extracted from the solution NMR-based structure of the GtCitA PASp (R93A). (*B*) Cα-Cβ secondary chemical shift plot for the C terminus of PASp variants in CitApc. The secondary shift transition at L154 is observed in context of TM helices. Assignments for residues succeeding L154 could not be obtained in solid-state NMR experiments. (*C*) Overlay of Kp CitA PASp crystal structures in citrate-free (blue) and citrate-bound (red) states. Upon citrate binding, the C-terminal β-strand is shortened by one residue at T128. Based on sequence alignment, L154 in Gt CitA PASp is structurally equivalent to T128 in Kp CitA and E168 in Ec DcuS. Residue numbering of crystallized PASp domains was taken from the crystal structures.

Fig. 5. Solid-state NMR spectra of *G. thermodenitrificans* CitApc. (*A*) PDSD spectra of Gt CitApc (R93A) in both citrate-free and -bound states (blue and red, respectively). Peaks corresponding to L154 are highlighted on either side of the diagonal for both states. (*B*) Enlargement of the highlighted Ser/Thr spectral region of citrate-free CitApc (R93A). Assignments corresponding to liquid-state data on isolated PASp (R93A) are indicated; S51 assignments vary between solution and solid state. Above diagonal: peak assignments in solid state, below diagonal: peak positions predicted from liquid-state NMR data. (*C*) Structural model of PASp (R93A), highlighting residues with Cα-Cβ chemical shift differences of more than 0.5 ppm between isolated PASp and PASp in context of TM helices.

Structural Features of PASp Are Consistent Between the Isolated Domain and PASp in Context of Membrane-Embedded CitApc. To investigate the signal transduction mechanism for membrane-embedded CitA, we used the Gt CitApc constructs containing both the extracytoplasmic and the cytoplasmic PAS domains connected to the TM helices. With CitApc embedded in 1,2-dimyristoyl–*sn*-glycero–3-phosphocholine (DMPC) liposomes, we were able to track structural changes in PASp in context of the TM environment. Solid-state NMR samples of wild-type CitApc and CitApc (R93A) with and without citrate were assigned using a combination of chemical shift-matching based on liquid-state data and de novo assignment using two- and three-dimensional solid-state NMR spectra (36). Peak positions in solid-state spectra [2D proton-driven spin diffusion (PDSD), 3D NCACB, NCOCA, and NCOCACB] were in a first step predicted from liquid-state NMR assignments and, where possible, transferred to solid-state peaks.

Starting from residues assigned that way, sequential assignments were carried out by matching Cα-Cβ resonances in 3D spectra that either yield intraresidual (NCACB) or interresidual (NCOCA, NCOCACB) correlations. From there, Cα and Cβ correlations can be used for side-chain assignment in PDSD spectra. C-terminal residues of PASp (succeeding L154) could not be assigned that way due to severe overlap of leucine residues in solid-state spectra (including L154-L155 correlations). In general, the agreement between liquid- and solid-state spectra is excellent, with carbon chemical shift deviations below 0.2 ppm for most resonances (Fig. 5). Isolated PASp, as well as PASp (R93A)$_{free}$ and PASp (R93A)$_{bound}$, are monomeric in solution (*SI Appendix*, Fig. S4). Whereas this result is in agreement with a previous characterization of CitA PASp from *K. pneumoniae* (34), PASp in context of the full-length receptor is likely to be dimeric, as predicted for a functional HK and determined for the homolog DcuS (37). This is reflected by the chemical shift perturbation at the dimerization interface in CitApc compared with monomeric isolated PASp (Fig. 5 *B* and *C*). Tracking changes in L154 chemical shifts in CitApc (R93A) is particularly interesting, as it can be seen as a reporter residue for the signaling states of PASp. Indeed, a transition from negative secondary shift, indicative of β-strand conformation, to positive secondary shift in the citrate-bound state is observed both in the PASp (R93A) construct (Fig. 4*A*) and also in CitApc (R93A) (Fig. 4*B*). The identity of the changes in chemical shifts in PASp and CitApc constructs in general and particularly of this reporter residue is remarkable. In summary, Gt CitA PASp (R93A) in context of the full-length protein is functional and in isolation recapitulates the structure of the citrate-bound wild type.

Structural Changes Beyond the C-Terminal End of the PASp Domain. We also noted remarkable structural changes in the PASc domain in the CitApc construct. The PASc domain can be prepared in the OFF and ON state only in the context of the CitApc construct, making it substantially more difficult to explore the conformational changes happening there upon citrate binding. Fig. 6 shows the secondary chemical shifts indicative of secondary structure change for a substantial number of residues. In addition, 12 Cα-Cβ cross-peaks visible in the PDSD experiment for the OFF state vanish upon citrate binding, indicating a much larger flexibility of the ON state compared with the OFF state.

Slowed-Down Citrate-Binding Kinetics of PASp in Context of TM Helices. The kinetics of citrate binding was investigated for isolated PASp (R93A) and the CitApc (R93A) construct. During the titration of the PASp (R93A) domain with citrate, the chemical shifts of the amides of the PASp domain shifted linearly with the citrate concentration, and even at half-stoichiometric concentration, the peaks were visible, although showing some line broadening compared with the free or bound state (Fig. 2*A*). This indicates fast exchange on the NMR time scale, as expected for a small molecule binding with high micromolar affinity to the isolated PASp (R93A) domain. In contrast, a PDSD experiment on a sample of CitApc (R93A) in liposomes with substoichiometric citrate added yields two discrete sets of peaks, corresponding to the

Fig. 6. The chemical shift differences between citrate-free and -bound states in the PASpc construct for the PASc domain are reported on the PASc sequence. The 0.4-ppm scale has been chosen according to the tolerance used to copy the liquid-state resonances on the solid-state NMR experiments.

citate-free and -bound states (Fig. 2B), i.e., slow exchange. To rule out temperature-dependent effects on binding kinetics and to better compare with PASp measurements carried out at 25 °C, CitApc (R93A) with substoichiometric citrate was measured at 7 °C and 21 °C. Although the overall quality of the spectrum is lower at 21 °C, peaks corresponding to citrate-free and -bound states of PASp are in slow exchange also at the higher temperature. Thus, the kinetics of citrate binding is vastly different for PASp (R93A) and CitApc (R93A). For fast exchange, the lower limit of the exchange rate can be determined from the peak with the largest chemical shift difference ($\Delta\nu$) and the additional line broadening at half-stoichiometric conditions ($\Delta\Gamma$) (*SI Appendix*) (38). The amide proton of residue I86 was identified to fulfill this condition, yielding from $\Delta\nu$ = 130.8 Hz and $\Delta\Gamma$ = 15.5 Hz a lower limit of k_{ex} = 1730 s^{-1}. For slow exchange, a lower limit for the exchange rate can be determined from the peak with the smallest chemical shift difference. For CitApc, the Cβ-Cδ_1 correlations of I86 were identified to fulfill this condition, specifically for the Cδ_1 chemical shift. With a Cδ_1 resonance frequency separation of 29.1 Hz in the ω_1 dimension (Fig. 2B), k_{ex} of CitApc (R93A) therefore has to be considerably slower than 29.1 s^{-1}. The ligand-binding kinetics thus is slowed down in context of the TM environment at least by a factor of 60, supporting the conjecture that the TM helix motion is linked to the citrate-binding–induced contraction of the PASp domain. Because the reduction of the off-rate by a factor of 60 could be caused by tighter binding of citrate we investigated citrate-binding–induced activation of the native CitA (*SI Appendix*, Fig. S6). Here, half-maximal induction of the CitA-dependent reporter *citC-lacZ* was observed at a concentration of 2 ± 0.5 mM citrate in bacteria containing CitA (R93A), resulting in a K_d of 2 ± 0.5 mM. By contrast, if the reduction of the off-rate observed in the CitApc construct was a result of a tighter binding of citrate, we would have expected a K_d of around 10 µM.

Discussion

PASp Contraction in the Membrane Context. Mechanistic models for the transmembrane signaling of two-component systems rely heavily on predictions from isolated domains. The contraction of the PASp domain upon citrate binding was observed in the crystal structures of Kp CitA PASp, but could so far not be established in the membrane context for any HK. In this work, we confirmed Kp CitA PASp structural rearrangements in Gt CitA PASp (R93A). This includes contraction of the central β-scaffold toward bound citrate (*SI Appendix*, Fig. S3A), as well as the shortening of the C-terminal β-strand at L154 (Fig. 4). Structures of other ligand-bound PAS domains from DcuS and DctB (39) reveal similar binding modes that are likely to be commonly used by PAS domains sensing small molecules (40). It is remarkable that the malate-bound structure of DcuS (39) shows residue E168 at the PASp-TM2 interface in a non–β-strand conformation as well. This residue is homologous to T128 in the Kp CitA PASp crystal structure and L154 in Gt CitA PASp. Thus, this residue can be taken as an indicator for conformational conversion of the PASp domain.

In contrast to earlier studies (26, 28), we were able to track structural rearrangements in PASp in context of the TM helices using CitApc in a native-like environment. Just like in isolated PASp, the contraction of the β-scaffold with the resulting shortening of the C-terminal β-strand is evident in CitApc from chemical shift changes. Thus, the structural alterations identified in isolated PASp (R93A) can be confirmed in context of the membrane environment using CitApc (R93A) as a model for the full-length HK (Figs. 3 and 5), with the caveat that no data are available at present on the full-length Gt CitA. It can therefore be concluded that the well-characterized structural reorganizations in isolated PAS domains are maintained in context of the TM arrangement and that the contraction of the PASp domain

upon citrate binding is established as the mechanical signal that is transmitted through the membrane.

For PAS and closely related double-PDC domains (a tandem arrangement of two PDC domains, with PDC being synonymous for extracytoplasmic PAS sensory domains) (39), experimental evidence hints toward either a piston model or a scissors-blade model (41, 42) for TM helix motions. Whereas these models are in most cases predicted from isolated domains, cysteine cross-linking in PhoQ (24) and water accessibility studies on DcuS (43) directly probe the TM segments. Bayesian modeling based on cross-linking data suggests a scissoring movement of TM helices for PhoQ, whereas water accessibility of both states of DcuS is in favor of a piston-type pull. Irrespective of the mechanistic model, however, a PAS domain rearrangement is mandatory for TM helix motions to occur and has in this work been confirmed with atomic resolution as a pull from PASp domain contraction in context of the TM environment. The remarkable structural similarities at the C terminus of the PASp domains due to ligand binding, i.e., shortening of the C-terminal β-strand, suggests a conserved activation mechanism for the CitA/DcuS family of HKs.

Kinetics of Signal Transduction upon PASp Activation. The binding kinetics of citrate is slowed down by at least a factor of 60 between the PASp domain in isolation and in the context of the membrane. This reduction is not caused by a tighter binding of TM-containing constructs compared with free PASp (K_d = 640 µM; Fig. S2), as shown in *SI Appendix*, Fig. S6, where full-length CitA was half-maximally activated with 2 mM citrate. This is expected when the contraction of the PASp domain induces the TM2 helices to move within the membrane and most probably also against TM1 helices. In addition, the motion of TM2 will also induce motion of the PASc domains. The structural rearrangement of these protein domains, whose details are yet unexplored, makes it plausible that the kinetics is slowed down dramatically. Indeed, there are considerable secondary chemical shift changes in the PASc domain in the CitApc construct in the OFF and ON state (Fig. 6). Furthermore, 12 amino acids whose Cα-Cβ cross-peaks were visible in the OFF state of the CitApc construct do not contribute any cross-peaks in the ON state, indicating vastly different dynamics of the same residues before and after activation. The observed change in binding kinetics is a strong indication that the contraction of PASp exerts a mechanical force on TM2, which triggers helix and cytosolic domain motions that yet have to be fully characterized. Whether there is cooperativity in binding or not could not be revealed in this study, because only one set of signals is observed during the titration, which is compatible with full cooperativity or no cooperativity. The latter would require, in addition, that the chemical shifts of the citrate-loaded PASp domain would not be affected when the other PASp domain was unloaded. Given the loose contacts between the two domains and the small chemical shifts induced between free PASp and PASp in the CitApc construct, complete absence of cooperativity cannot be ruled out. In conclusion, a combination of solid- and solution-state NMR spectroscopy combined with structures determined from X-ray crystallography can be used in conjunction with a reporter gene assay to monitor structural rearrangements in HKs. This allows confirming PASp contraction in the membrane context as the crucial mechanical signal that is transmitted through the membrane.

Materials and Methods

Protein Expression and Purification. Plasmids containing CitA constructs were generated using the strains and plasmids listed in *SI Appendix, Table S2* and standard procedures (44). PCR amplification and vector ligation were carried out as detailed in *SI Appendix, SI Materials and Methods*. Expression of Gt CitA PASp and CitApc samples, as well as purification via immobilized metal affinity chromatography and size exclusion chromatography (SEC), are described in detail in *SI Appendix, SI Materials and Methods*. Samples of Gt CitA PASp were dialyzed over night against NMR buffer (20 mM sodium phosphate pH 6.5, 50 mM NaCl) and concentrated to 1.4–1.8 mM, followed by addition of 0.01% (wt/vol) sodium azide.

Gt CitApc samples were purified via immobilized metal affinity chromatography and SEC as described in *SI Appendix, SI Materials and Methods*. In short, Gt CitApc was extracted from cell pellets using buffer supplemented with Triton X-100, which was exchanged to laurydimethylamine-oxide (LDAO) on Ni-NTA resin. After SEC, LDAO-solubilized samples were reconstituted into 1,2-dimyristoyl-*sn*-glycero-3-phosphocholine (DMPC) liposomes. Citrate-bound samples of CitApc (R93A) were purified with excess citrate in all buffers. Reconstituted samples were pelleted via ultracentrifugation and packed into 4-mm and 3.2-mm solid-state NMR rotors.

Reporter Gene Assays. In vivo activation (β-galactosidase) assays were carried out in microtiter plates as described elsewhere (28), using strains IMW548 or IMW549 (45) with plasmid pMW1653 encoding CitB$_{Ec}$ and, additionally, plasmid pMW1652 (46) encoding CitA$_{Gt}$ or pMW2304 encoding CitA$_{Gt}$(R93A) (*SI Appendix*, Table S2).

NMR Spectroscopy. PASp variants were assigned using triple-resonance spectra, listed in *SI Appendix, SI Materials and Methods*, recorded on Bruker spectrometers ranging from 400 to 900 MHz at 25 °C. Chemical shift assignments for the citrate-free and citrate-bound variants are listed in *SI Appendix*, Tables S3 and S4, respectively. Solid-state NMR samples of CitApc reconstituted in DMPC were measured on Bruker spectrometers (800 and 850 MHz) at 7–9 °C. Spectra were processed with NMRpipe (47) and assigned using Collaborative Computing Project for NMR (CCPN) analysis (48). Chemical shift assignments for the PASpc construct in the citrate-free and citrate-bound state are listed in *SI Appendix*, Tables S5 and S6, respectively. K_d of PASp (R93A) was determined from a citrate titration using global fitting to the equation, reported in ref. 31, of isolated proton chemical shifts in ^{1}H-^{15}N-HSQC experiments recorded at 400 MHz (32, 33). Secondary chemical shifts (35) were calculated using random coil chemical shifts (49, 50). NMR structural models (*SI Appendix*, Table S1) were calculated from NOE-, RDC-, and hydrogen bond-restraints using ARIA2 (51). The rmsd values between the Gt CitA PASp and the Kp CitA PASp structures were calculated averaging the single rmsd value between one structure of the NMR-based ensemble and the crystal structure.

1. Parkinson JS (1993) Signal transduction schemes of bacteria. *Cell* 73(5):857–871.
2. Stock AM, Robinson VL, Goudreau PN (2000) Two-component signal transduction. *Annu Rev Biochem* 69:183–215.
3. Grebe TW, Stock JB (1999) The histidine protein kinase superfamily. *Adv Microb Physiol* 41:139–227.
4. Hoch JA (2000) Two-component and phosphorelay signal transduction. *Curr Opin Microbiol* 3(2):165–170.
5. Stock JB, Surette MG, Levit M, Park P (1995) Two-component signal transduction systems: Structure-function relationships and mechanisms of catalysis. *Two-Component Signal Transduction*, eds Hoch JA, Silhavy TJ (ASM Press, Washington, D.C.), pp 25–51.
6. Parkinson JS, Kofoid EC (1992) Communication modules in bacterial signaling proteins. *Annu Rev Genet* 26:71–112.
7. Casino P, Rubio V, Marina A (2010) The mechanism of signal transduction by two-component systems. *Curr Opin Struct Biol* 20(6):763–771.
8. Cheung J, Hendrickson WA (2010) Sensor domains of two-component regulatory systems. *Curr Opin Microbiol* 13(2):116–123.
9. Gao R, Stock AM (2009) Biological insights from structures of two-component proteins. *Annu Rev Microbiol* 63:133–154.
10. Mascher T, Helmann JD, Unden G (2006) Stimulus perception in bacterial signal-transducing histidine kinases. *Microbiol Mol Biol Rev* 70(4):910–938.
11. Perry J, Koteva K, Wright G (2011) Receptor domains of two-component signal transduction systems. *Mol Biosyst* 7(5):1388–1398.
12. Stewart RC (2010) Protein histidine kinases: Assembly of active sites and their regulation in signaling pathways. *Curr Opin Microbiol* 13(2):133–141.
13. Wang C, et al. (2013) Mechanistic insights revealed by the crystal structure of a histidine kinase with signal transducer and sensor domains. *PLoS Biol* 11(2):e1001493.
14. Tan K, et al. (2014) Sensor domain of histidine kinase KinB of Pseudomonas: A helix-swapped dimer. *J Biol Chem* 289(18):12232–12244.
15. Moore JO, Hendrickson WA (2012) An asymmetry-to-symmetry switch in signal transmission by the histidine kinase receptor for TMAO. *Structure* 20(4):729–741.
16. Neiditch MB, et al. (2006) Ligand-induced asymmetry in histidine sensor kinase complex regulates quorum sensing. *Cell* 126(6):1095–1108.
17. Bhate MP, Molnar KS, Goulian M, DeGrado WF (2015) Signal transduction in histidine kinases: Insights from new structures. *Structure* 23(6):981–994.
18. Biemann HP, Koshland DE, Jr (1994) Aspartate receptors of Escherichia coli and Salmonella typhimurium bind ligand with negative and half-of-the-sites cooperativity. *Biochemistry* 33(3):629–634.
19. Chervitz SA, Falke JJ (1996) Molecular mechanism of transmembrane signaling by the aspartate receptor: A model. *Proc Natl Acad Sci USA* 93(6):2545–2550.
20. Cheung J, Hendrickson WA (2009) Structural analysis of ligand stimulation of the histidine kinase NarX. *Structure* 17(2):190–201.
21. Scheu PD, Kim OB, Griesinger C, Unden G (2010) Sensing by the membrane-bound sensor kinase DcuS: Exogenous versus endogenous sensing of C(4)-dicarboxylates in bacteria. *Future Microbiol* 5(9):1383–1402.
22. Ottemann KM, Xiao W, Shin Y-K, Koshland DE, Jr (1999) A piston model for transmembrane signaling of the aspartate receptor. *Science* 285(5434):1751–1754.
23. Sevvana M, et al. (2008) A ligand-induced switch in the periplasmic domain of sensor histidine kinase CitA. *J Mol Biol* 377(2):512–523.
24. Molnar KS, et al. (2014) Cys-scanning disulfide crosslinking and Bayesian modeling probe the transmembrane signaling mechanism of the histidine kinase, PhoQ. *Structure* 22(9):1239–1251.
25. Diensthuber RP, Bommer M, Gleichmann T, Möglich A (2013) Full-length structure of a sensor histidine kinase pinpoints coaxial coiled coils as signal transducers and modulators. *Structure* 21(7):1127–1136.
26. Etzkorn M, et al. (2008) Plasticity of the PAS domain and a potential role for signal transduction in the histidine kinase DcuS. *Nat Struct Mol Biol* 15(10):1031–1039.
27. Kneuper H, et al. (2005) The nature of the stimulus and of the fumarate binding site of the fumarate sensor DcuS of Escherichia coli. *J Biol Chem* 280(21):20596–20603.
28. Monzel C, Degreif-Dünnwald P, Gröpper C, Griesinger C, Unden G (2013) The cytoplasmic PASC domain of the sensor kinase DcuS of *Escherichia coli*: Role in signal transduction, dimer formation, and DctA interaction. *MicrobiologyOpen* 2(6):912–927.
29. Altschul SF, Gish W, Miller W, Myers EW, Lipman DJ (1990) Basic local alignment search tool. *J Mol Biol* 215(3):403–410.
30. Gerharz T, Reinelt S, Kaspar S, Scapozza L, Bott M (2003) Identification of basic amino acid residues important for citrate binding by the periplasmic receptor domain of the sensor kinase CitA. *Biochemistry* 42(19):5917–5924.
31. Montaville P, et al. (2008) The PIP2 binding mode of the C2 domains of rabphilin-3A. *Protein Sci* 17(6):1025–1034.
32. Auguin D, et al. (2004) Structural basis for the co-activation of protein kinase B by T-cell leukemia-1 (TCL1) family proto-oncoproteins. *J Biol Chem* 279(34):35890–35902.
33. McKay RT, Tripet BP, Pearlstone JR, Smillie LB, Sykes BD (1999) Defining the region of troponin-I that binds to troponin-C. *Biochemistry* 38(17):5478–5489.
34. Kaspar S, et al. (1999) The periplasmic domain of the histidine autokinase CitA functions as a highly specific citrate receptor. *Mol Microbiol* 33(4):858–872.
35. Metzler WJ, et al. (1993) Characterization of the three-dimensional solution structure of human profilin: 1H, 13C, and 15N NMR assignments and global folding pattern. *Biochemistry* 32(50):13818–13829.
36. Shi C, et al. (2014) BSH-CP based 3D solid-state NMR experiments for protein resonance assignment. *J Biomol NMR* 59(1):15–22.
37. Scheu PD, et al. (2010) Oligomeric sensor kinase DcuS in the membrane of *Escherichia coli* and in proteoliposomes: Chemical cross-linking and FRET spectroscopy. *J Bacteriol* 192(13):3474–3483.
38. Anet FAL (1964) Ring inversion in Cycloheptatriene. *J Am Chem Soc* 86(3):458–460.
39. Cheung J, Hendrickson WA (2008) Crystal structures of C4-dicarboxylate ligand complexes with sensor domains of histidine kinases DcuS and DctB. *J Biol Chem* 283(44):30256–30265.
40. Henry JT, Crosson S (2011) Ligand-binding PAS domains in a genomic, cellular, and structural context. *Annu Rev Microbiol* 65:261–286.
41. Matthews EE, Zoonens M, Engelman DM (2006) Dynamic helix interactions in transmembrane signaling. *Cell* 127(3):447–450.
42. Lowe EC, Baslé A, Czjzek M, Firbank SJ, Bolam DN (2012) A scissor blade-like closing mechanism implicated in transmembrane signaling in a Bacteroides hybrid two-component system. *Proc Natl Acad Sci USA* 109(19):7298–7303.
43. Monzel C, Unden G (2015) Transmembrane signaling in the sensor kinase DcuS of Escherichia coli: A long-range piston-type displacement of transmembrane helix 2. *Proc Natl Acad Sci USA* 112(35):11042–11047.
44. Green MR, Sambrook J (2012) *Molecular Cloning: A Laboratory Manual* (Cold Spring Harbor Lab Press, Cold Spring Harbor, NY), 4th Ed, p 2028.
45. Scheu PD, et al. (2012) CitA/CitB two-component system regulating citrate fermentation in Escherichia coli and its relation to the DcuS/DcuR system in vivo. *J Bacteriol* 194(3):636–645.
46. Graf S, et al. (2015) CitA (citrate) and DcuS (C4-dicarboxylate) sensor kinases in thermophilic *Geobacillus kaustophilus* and *G. thermodenitrificans*. *Microbiology* 162(1):127–37.
47. Delaglio F, et al. (1995) NMRPipe: A multidimensional spectral processing system based on UNIX pipes. *J Biomol NMR* 6(3):277–293.
48. Vranken WF, et al. (2005) The CCPN data model for NMR spectroscopy: Development of a software pipeline. *Proteins* 59(4):687–696.
49. Wang Y, Jardetzky O (2002) Investigation of the neighboring residue effects on protein chemical shifts. *J Am Chem Soc* 124(47):14075–14084.
50. Wang Y, Jardetzky O (2002) Probability-based protein secondary structure identification using combined NMR chemical-shift data. *Protein Sci* 11(4):852–861.
51. Rieping W, et al. (2007) ARIA2: automated NOE assignment and data integration in NMR structure calculation. *Bioinformatics* 23(3):381–382.